Correlative 3D-Imaging of *Pipistrellus* Penis Micromorphology: Validating Quantitative MicroCT Images with Undecalcified Serial Ground Section Histomorphology

Anna Nele Herdina,[1]* Hanns Plenk Jr.,[2] Petr Benda,[3,4] Peter H. C. Lina,[5] Barbara Herzig-Straschil,[6] Helge Hilgers,[7] and Brian D. Metscher[1]

[1]*Department of Theoretical Biology, Faculty of Life Sciences, University of Vienna, Althanstrasse 14, A-1090 Vienna, Austria*
[2]*Bone and Biomaterials Research, Institute of Histology and Embryology, Medical University of Vienna, Schwarzspanierstrasse 17, A-1090 Vienna, Austria*
[3]*Department of Zoology, National Museum (Natural History), Václavské náměstí 68, CZ-115 79 Praha 1, Czech Republic*
[4]*Department of Zoology, Faculty of Science, Charles University in Prague, Viničná 7, CZ-128 44 Praha 2, Czech Republic*
[5]*Department of Terrestrial Zoology, Naturalis Biodiversity Center, P.O. Box 9517, 2300 RA Leiden, the Netherlands*
[6]*Mammal Collection, Natural History Museum Vienna, Burgring 7, A-1010 Vienna, Austria*
[7]*Department of Integrative Zoology, Faculty of Life Sciences, University of Vienna, Althanstrasse 14, A-1090 Vienna, Austria*

ABSTRACT Detailed knowledge of histomorphology is a prerequisite for the understanding of function, variation, and development. In bats, as in other mammals, penis and baculum morphology are important in species discrimination and phylogenetic studies. In this study, nondestructive 3D-microtomographic (microCT, μCT) images of bacula and iodine-stained penes of *Pipistrellus pipistrellus* were correlated with light microscopic images from undecalcified surface-stained ground sections of three of these penes of *P. pipistrellus* (1 juvenile). The results were then compared with μCT-images of bacula of *P. pygmaeus*, *P. hanaki*, and *P. nathusii*. The Y-shaped baculum in all studied *Pipistrellus* species has a proximal base with two club-shaped branches, a long slender shaft, and a forked distal tip. The branches contain a medullary cavity of variable size, which tapers into a central canal of variable length in the proximal baculum shaft. Both are surrounded by a lamellar and a woven bone layer and contain fatty marrow and blood vessels. The distal shaft consists of woven bone only, without a vascular canal. The proximal ends of the branches are connected with the tunica albuginea of the corpora cavernosa via entheses. In the penis shaft, the corpus spongiosum-surrounded urethra lies in a ventral grove of the corpora cavernosa, and continues in the glans under the baculum. The glans penis predominantly comprises an enlarged corpus spongiosum, which surrounds urethra and baculum. In the 12 studied juvenile and subadult *P. pipistrellus* specimens the proximal branches of the baculum were shorter and without marrow cavity, while shaft and distal tip appeared already fully developed. The present combination with light microscopic images from one species enabled a more reliable interpretation of histomorphological structures in the μCT-images from all four *Pipistrellus* species. J. Morphol. 276:695–706, 2015. © 2015 Wiley Periodicals, Inc.

KEY WORDS: Vespertilionidae; Chiroptera; male reproductive organ; X-ray microtomography; iodine staining; bone

INTRODUCTION

Correlative imaging is a well-established approach in many radiological and light- and electron-microscopic studies on diverse topics and materials. Since the invention of radiographic

Correction added on May 6, 2015, after first online publication: LIETERATURE CITED changed to LITERATURE CITED.

Contract grant sponsor: Partial funding for this study was provided by a Marietta Blau Fellowship (ICM-2011-03590) for A.N.H. by the Austrian Federal Ministry of Science and Research and the Austrian Agency for International Cooperation in Education and Research (OeAD), by a PhD Completion Grant for A.N.H. by the Faculty of Life Sciences, University of Vienna, and by a grant for P.B. by the Ministry of Culture of the Czech Republic (# DKRVO 2014/14, 00023272).

*Corresponding author: Anna Nele Herdina; Department of Theoretical Biology, Faculty of Life Sciences, University of Vienna, Althanstrasse 14, A-1090 Vienna, Austria.
E-mail: annanele.herdina@univie.ac.at

Received 9 July 2014; Revised 11 January 2015; Accepted 17 January 2015.

Published online 21 February 2015 in Wiley Online Library (wileyonlinelibrary.com).
DOI 10.1002/jmor.20372

© 2015 WILEY PERIODICALS, INC.

techniques, it has been standard to present them in combination with histomorphological findings in anatomical textbooks. Combining microtomographic (microCT, μCT) imaging with other 2D or 3D-imaging methods adds information from cell and tissue level histomorphology to the overall three dimensional structures. Because of the inherent physical limitations of each method, a correlative approach can yield a significantly broader range of information (Handschuh et al., 2013). Thus, correlative imaging was applied to the further evaluation of bat baculum histomorphology in the present study.

Combining nondestructive, quantitative μCT-imaging with classical histomorphological techniques enables us to take advantage of the possibilities of both methods while avoiding some of the limitations of each. 2D and 3D-images derived from μCT-scans can contain information on cell and tissue scales, and validating this information with light microscopic evaluation of undecalcified, surface-stained ground sections of the same specimen in a corresponding orientation is useful to corroborate findings. Once a structure or tissue type has been calibrated in this way, further conclusions can be drawn from μCT-images of other specimens and even specimens of different species. Thus the time-consuming and destructive processing of a small number of samples can be used to validate results of a larger number of nondestructive μCT-images, allowing us to study specimens which are rare in scientific collections in numbers sufficient to evaluate individual and geographic variation of the respective traits. Additionally, 3D-renderings of μCT-images contain information that is difficult or impossible to glean even from serial histological sections. In particular, complicated three-dimensional structures are much easier to study in an interactive 3D-visualization. Virtual 2D-sections from μCT-scans can be shown in any orientation and combination, and they constitute an independent data set that can be useful in any further studies of the imaged specimen.

The main object of this study, the baculum (penial bone, os penis, os priapi, os glandis), is an extra-skeletal or heterotopic bone present in the penis of many species of the mammalian orders Carnivora, Chiroptera, Eulipotyphla, Primates, and Rodentia (Patterson and Thaeler, 1982). The size of the baculum in relation to the size of the penis varies between species, as does the position of the baculum within the penis (Meisenheimer, 1921; Patterson, 1983). While the shape of the baculum usually does show similarities between the species of a genus, it is often distinctly different between closely related species (in bats, see e.g., Topál, 1958; Hill and Harrison, 1987). Thus, due to its usefulness as a taxonomic character (Thomas, 1915; Burt, 1936), the macromorphology of bat bacula has been studied extensively. The position of the baculum in context with the surrounding erectile tissues has been studied histologically in several bat species (Gilbert, 1892; Ercolani, 1868 cited in Matthews, 1937; Ryan, 1991a, 1991b), but the histomorphological features of the penis bone have not been described in particular.

In a more recent approach, our research group has already applied correlative 2D and 3D-imaging to describe baculum histomorphology in three species of the bat genus *Plecotus* (Herdina, 2008; Herdina et al., 2010a). As suggested at least for *Plecotus*, the micromorphological traits of shape and position of the medullary cavity in the baculum and the position and number of nutrient foramina (where blood vessels enter the bone from the periosteum going into Volkmann's canals) may prove useful for species discrimination (Herdina, 2008). Research on penis bone histomorphology could also add valuable information about the development of the baculum and its mechanical function. So far, studies on baculum histomorphology and development have been conducted mainly in rodents (e.g., Ruth, 1934; Friley Jr, 1949; Callery, 1951; Iguchi et al., 1990; Murakami and Mizuno, 1984, 1986; Retterer, 1887; Spotorno, 1992; Weiss et al., 2012) and in carnivores (e.g., Petrides, 1950; Miller et al., 1998; Albayrak et al., 2008; Schwery et al., 2011).

We have continued to study the histomorphological traits of penes and bacula not only for their value in bat species discrimination (Herdina et al., 2014), but also for determining specific mechanical functions of the penis bone in bats (Herdina et al., 2015). In the scope of these ongoing studies, we have concentrated on the *Pipistrellus pipistrellus* species complex (Chiroptera, Vespertilionidae), which is a valuable model system for studying cryptic diversity in European bats (*Davidson*-Watts et al., 2006; Hulva et al., 2010). In the present study, we have i) refined current correlative 2D and 3D-imaging techniques by validating the histomorphology in virtual section images of non-invasive μCT with corresponding images of serial surface-stained undecalcified ground sections; ii) established a histomorphological basis for functional studies of the baculum in the *Pipistrellus pipistrellus* species complex; and iii) collected and interpreted preliminary histomorphological data on *P. pipistrellus* baculum development.

MATERIAL AND METHODS

The specimens for this study are deposited at the National Museum (Natural History) Prague, Czech Republic: *Pipistrellus pipistrellus* (Schreber, 1774) ($n = 30$: NMP 48060, NMP 48061, NMP 48872, NMP 48981, NMP 48982, NMP 48983, NMP 48984, NMP 90014, NMP 90016, NMP 90017, NMP 90791, NMP 90832, NMP 90839, NMP 90840, NMP 94541, NMP 94542, NMP 94544, NMP 94546, NMP LE 19, NMP LE 20, NMP LE 21, NMP LE 22, NMP LE 24, NMP LE 26, NMP LE 101, NMP LE 102, NMP LE 103, NMP LE 105, NMP LE 118,

TABLE 1. Measurements on the bacula of juvenile and subadult P. pipistrellus s.l., and adult P. pipistrellus s.str., P. pygmaeus, P. hanaki, and P. nathusii

	Projected length $\bar{x}$ (range)	Projected width $\bar{x}$ (range)	Projected height $\bar{x}$ (range)
P. pipistrellus ($n=5$) juvenile	1267.3 µm (1185.9–1377.6)	210.1 µm (182.7–237.9)	230.4 µm (205.2–267.8)
P. pipistrellus ($n=4$) younger subadult	1364.5 µm (1253.5–1422.4)	210.2 µm (166.2–230.8)	276.6 µm (205.2–322.3)
P. pipistrellus ($n=3$) older subadult	1570.3 µm (1541.8–1589.1)	287.9 µm (236.9–265.6)	333.2 µm (317.8–354.3)
P. pipistrellus ($n=30$) adult	1687.7 µm (1531.5–1835.4)	371.7 µm (285.8–417.9)	366.9 µm (309.9–458.6)
P. pygmaeus ($n=24$) adult	1559.3 µm (1420.6–1767.8)	325.9 µm (281.5–397.3)	351.9 µm (296.0–510.7)
P. hanaki ($n=9$) adult	1478.7 µm (1319.1–1762.2)	315.1 µm (272,0–393.5)	294.5 µm (243.0–387.9)
P. nathusii ($n=4$) adult	1375.5 µm (1292.0–1447.5)	399.4 µm (367.9–430.8)	246.4 µm (241.1–259.6)

Arithmetic mean ($\bar{x}$) and range of projected length, width, and height.

NMP LE 212); *P. pygmaeus* (Leach, 1825) ($n=24$: NMP 47946, NMP 48738, NMP 49016, NMP 49021, NMP 49030, NMP 49040, NMP 90011, NMP 90138, NMP 90408, NMP 90413, NMP 90414, NMP 90416, NMP 90417, NMP 90420, NMP 90875, NMP 90876, NMP 90877, NMP 90879, NMP 90881, NMP 90885, NMP 90886, NMP 90887, NMP 90888, NMP 90889); *P. hanaki* Hulva & Benda, 2004 ($n=9$: NMP 49891, NMP 49902, NMP 92323, NMP 92344, NMP 92349, NMP 92350, NMP 92351, NMP 92352, NMP 92353), all of them genetically identified; the from Naturalis Biodiversity Center, Leiden, The Netherlands (will be vouchered at the Natural History Museum Vienna): *P. pipistrellus* (Schreber, 1774) *sensu lato* (*s.l.*) ($n=5$: ANH2013/003, ANH2013/021, two of them subadult: ANH2013/006, ANH2013/012, one juvenile: ANH2013/020); *P. nathusii* (Keyserling and Blasius, 1839) ($n=3$: ANH2013/009, ANH2013/019, ANH2013/026); and the Natural History Museum Vienna, Austria: *P. pipistrellus* (Schreber, 1774) *s.l.* ($n=30$: NMW AM1993/071, NMW AM1993/073, NMW 11946, NMW 27481, NMW 28334, NMW 28335, NMW 28340, NMW 50730, NMW 50904, NMW 51507, NMW 52177, NMW 52186, NMW 52790, NMW 52795, NMW 63018, NMW 64076, NMW 64876, NMW 65246, NMW 66144, NMW 66478, NMW 66589, five of them subadult: NMW 64875, NMW 35459, NMW 64075, NMW 51057, NMW 52183, four juvenile: NMW F1246, NMWnoninvent1, NMWnoninvent2, NMW 66530); *P. nathusii* (Keyserling and Blasius, 1839) ($n=1$: NMW 66478). The specimens were whole bats or resected penes (flaccid), preserved in 70% ethanol. All histological ground-sections and all image stacks from µCT-imaging will be vouchered at the museums with the respective specimens, available under the specimen numbers. The image data and metadata will be accessible through the responsible museums.

MicroCT-imaging was used for histomorphological and histometrical evaluation of the bacula of all four *Pipistrellus* species (*Pipistrellus pipistrellus*, $n=65$; *P. pygmaeus*, $n=24$; *P. hanaki*, $n=9$; *P. nathusii*, $n=4$). The penes of whole bats, preserved in ethanol, were µCT-scanned unstained. The bats were mounted intact in plastic sample vials in 70% ethanol. Resected bat penes (*P. pipistrellus s.l.*, $n=12$; *P. nathusii* $n=4$) were scanned unstained and then scanned again after iodine staining for soft tissues. For contrast staining, they were transferred to 100% ethanol via ascending ethanol concentrations, and stained with 1% (w/v) elemental iodine in 100% ethanol (I2E; Metscher, 2009a; Herdina et al., 2010a; Metscher, 2011) for at least 14 h, up to several days. Before scanning, the samples were transferred back to 100% ethanol for at least one hour to improve contrast. Resected bat penes were mounted in polypropylene micropipette tips (heat-sealed and filled with 70% or 100% ethanol, Metscher, 2009a) and sealed with Parafilm.

MicroCT-imaging was performed using an Xradia MicroXCT system (www.xradia.com), with a microfocus tungsten source, secondary optical magnification of the scintillator images, and a 2k × 2k cooled CCD camera. Projection images were collected every 0.25° over a rotation of 180° (plus the cone angle Metscher, 2009b, 2011) with 2×2 pixel binning, at 4× or 10× optical magnification, exposure times of 4–10 sec, and source voltages of 40–60 kVp at 4–8 W. Tomographic virtual sections were reconstructed using the XMReconstructor software (version 8.1) supplied with the Xradia MicroXCT system, resulting in reconstructed isotropic voxel sizes of 2.0–2.5 µm.

Virtual sections from the reconstructed volume images were evaluated and measured. On virtual thick sections projected baculum length, width, and height were measured of adult *P. pipistrellus s.str.* ($n=30$), *P. pygmaeus* ($n=24$), *P. hanaki* ($n=9$), and *P. nathusii* ($n=4$); and juvenile ($n=5$) and subadult ($n=7$) *P. pipistrellus s.l.* (Table 1). In the automatically reconstructed µCT-images, bone and soft tissues were segmented (subvolumes representing different tissues selected) manually using Amira 5.4.5 to create 3D-models (Herdina et al., 2010b, 2015; Metscher, 2009a, 2009b, 2011).

The penes of three *Pipistrellus pipistrellus* (one of them juvenile), which had been iodine stained and µCT-scanned, were prepared for light microscopic evaluation of serial surface-stained undecalcified ground sections (Plenk Jr., 1986; Herdina et al., 2010b). The penes were transferred from 100% ethanol to acetone:ethanol (1:1; 100%), then 100% ethanol, and infiltrated with pure methylmethacrylate. Subsequently, they were embedded in glass containers in a mixture of 800 ml methylmethacrylate, 100 ml Plastoid N, and 15 g benzoyl peroxide in a water bath (28–32°C) for 4 days. The polymerized blocks were hardened at 50°C in a heating cabinet overnight. The blocks were trimmed roughly on a band saw (Emco GmbH, 5400 Hallein, Austria) and then sectioned close to the surface of the embedded penis on a low speed saw (Buehler Isomet low-speed saw; Evanston, IL). One specimen block each was cut and ground longitudinally, starting from either the dorsal or ventral side of the penis. The specimen block from the juvenile bat was cross-sectioned, starting from the proximal end of the glans penis. The resulting surfaces of the respective specimen blocks were polished and glued (CA8 Pronto instant adhesive, 3M) to a plexiglass slide. A 3 mm thick section of was cut parallel to this surface. This thick section was ground (EXAKT-Type AW 10, EXAKT Advanced Technologies GmbH, D-22851 Norderstedt, Germany; 1,000-grit and 4,000-grit sandpaper) until the skin of the penis was exposed. This surface and consecutive ground surfaces were polished (Buehler Minimet Polisher; Evanston, IL; alumina polishing powder, particle size 1.0 µm) for surface staining. Before staining they were treated for 2 min in 0.1% formic acid in distilled water (A. dest.), then rinsed in A. dest., stained 20–40 min in freshly prepared Giemsa-solution (Merck GmbH, Darmstadt, Germany), differentiated in 100 ml A. dest. with five drops of glacial acetic acid, and rinsed again in A. dest. Some sections were contrasted with pararosaniline (method: Barbara Rendl and Astrid Haase, personal communication). Dried surfaces were evaluated without cover slips by light microscopy (Nikon E 600) and photographed (Nikon J1, Nikon, Japan).

RESULTS

Evaluation of µCT virtual sections and 3D-renderings showed that the bacula of *Pipistrellus pipistrellus*, *P. pygmaeus*, *P. hanaki*, and

Fig. 1. Examples of bacula of *P. pipistrellus* (NMW 66144), *P. pygmaeus* (NMP 48738), *P.hanaki* (NMP 92349), and *P. nathusii* (NMW 66479). Left to right; 3D surface renderings of μCT-images, scaled to the same size to compare shape only; for sizes see Table 1) in dorsal view (upper row) and lateral view (lower row). Scale bars: 200μm. Medullary cavity and canals shown in orange.

P. nathusii are all Y-shaped in dorsal view (Fig. 1). The two branches of the base are slender where they split, but widen considerably towards the proximal ends. The angle of this branching shows interspecific and intraspecific variations (Herdina et al., 2014). In all four *Pipistrellus* species studied, the shaft of the baculum is long and slender in proportion to the base. The small distal tip of the baculum is forked and directly encases the upper half of the external urethral orifice within the glans penis.

In lateral view (Fig. 1), the bacula of *P. pipistrellus*, *P. pygmaeus*, and *P. hanaki* show a pronounced dorsoventral curve, with the broader base tapering towards the narrow tip. The curve shape in these three species shows considerable individual variation. *P. nathusii* bacula are also curved dorsoventrally, but bend back dorsally near the distal end of the shaft. Table 1 contains the mean and range of baculum measurements.

MicroCT-images also show the position of a medullary cavity and the course of a medullary/vascular canal and Volkmann's canals in the bacula (Fig. 1). In most specimens, both widened proximal ends of the branches of the baculum contain marrow cavities, which can be very large and can have several Volkmann's canals. A narrower marrow canal leads to a central Haversian canal in the proximal portion of the baculum shaft. In all four *Pipistrellus* species, considerable individual variation was observed in the length of the canals, the number and position of the nutrient foramina, and further Volkmann's canals sometimes branching off the Haversian canal in the shaft. In three specimens of *P. hanaki*, a medullary cavity was completely absent.

Light microscopic histology of undecalcified ground sections of *P. pipistrellus* penes showed that the proximal branches (base) of the baculum consist of a layer of woven bone with densely packed irregular osteocytes around an inner layer of lamellar bone (Figs. 2–4). In the woven bone layer, the tunica albuginea connects the corpora cavernosa to the baculum with fibrocartilage-like cells (Figs. 3 and 4). Such a connection is identified as an enthesis (Benjamin et al., 1986). The layer of lamellar bone encases the medullary cavity, which is filled with fatty bone marrow and blood vessels (Figs. 2–4). The proximal part of the baculum shaft consists of a tubular bone with a central medullary or vascular canal (of variable length and morphology), surrounded by concentric lamellar bone with regularly spaced, oval shaped osteocytes (Figs. 4 and 5). This inner lamellar layer of the proximal shaft is in most places separated from the peripheral subperiosteal woven bone by a distinct cement line (Figs. 4 and 5). The distal part of the baculum shaft with its slender and forked tip consists of woven bone only (Fig. 6).

The thick fibrous tunicae albugineae of the paired corpora cavernosa are merged for most of the length of the penis shaft (Figs. 2 and 3). Where they merge, a thinner continuation of the combined tunicae albugineae forms the incomplete septum pectinatum, allowing blood lacunae to communicate. Between the blood lacunae a network of more fibrous trabeculae can be seen, which connect to the tunica albuginea (Figs. 2 and 3). In μCT virtual cross sections, the corpora cavernosa are shaped like a thick horseshoe, with a ventral groove along their length. At the distal end, the gradually thinning tunica albuginea continues into the fibrous layer of the dorsal periosteum of the baculum (Figs. 2–4).

The urethra is lined with urethral mucosa, a multilayered epithelium, and surrounded by the

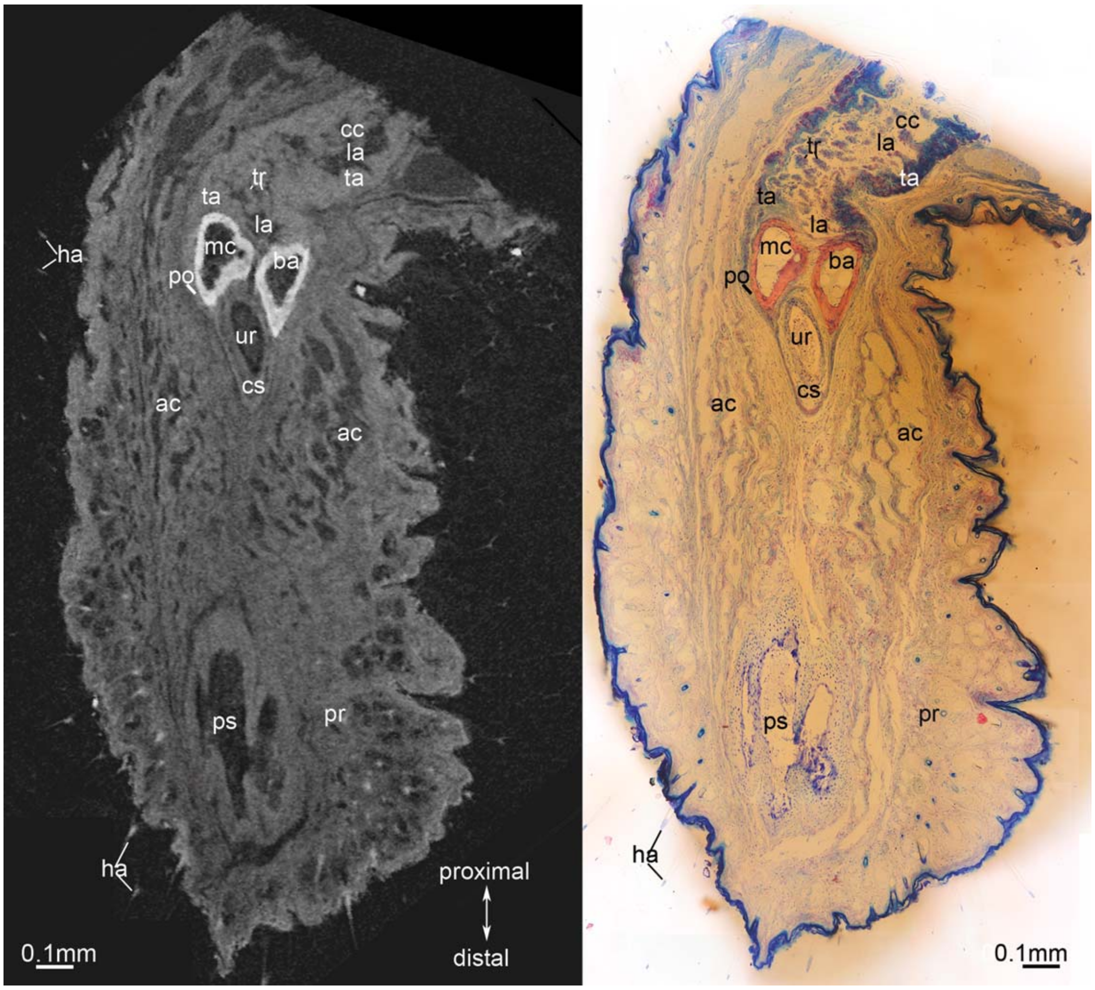

Fig. 2. Ventral view of a *P. pipistrellus* (NMW 52177) penis (distal part of the shaft and glans), surface-stained ground section (right; Giemsa stain and pararosaniline; photographs stitched with Adobe Photoshop CS6), comparing the corresponding μCT virtual section (left; iodine stained, overview scan) of the same specimen; ac: accessory swelling tissue, ba: baculum, cc: corpora cavernosa, cs: corpus spongiosum, ha: hair, la: blood lacunae (in the corpora cavernosa), mc: medullary cavity (within the baculum) with fatty bone marrow and blood vessels, po: periosteum, pr: preputium, ps: preputial sac, ta: tunica albuginea (of the corpora cavernosa), tr: trabeculae (in the corpora cavernosa), ur: urethra.

corpus spongiosum (Figs 2–5 and especially 6). Proximally, the urethra lies in the ventral grove of the merged corpora cavernosa, and then continues under the baculum towards the forked distal end (Fig. 5). In the glans penis, the corpus spongiosum becomes more voluminous and completely envelops the urethra and the baculum. The corpus spongiosum is also enveloped in a fibrous layer, but thinner than the tunica albuginea of the corpora cavernosa (Fig. 6). Finally, the urethra ends with the external urethral orifice, which is beveled like the tip of a hypodermic needle, its dorsal half being enclosed by the forked tip of the baculum (Figs. 5 and 6). The preputium is thick and vascular (Figs. 2, 5, and 6). The inner, visceral surface of the preputium and the skin of the glans consist of a stratified squamous epithelium (the cell nuclei of which are visible in Fig. 6), as in most mammals (Banks, 1993). The preputium contains accessory swelling tissue, a subcutaneous layer of fat, and sebaceous glands (Fig. 6). The transition from the normal skin of the penis occurs about where the corpus spongiosum widens. The preputial sac is filled with abundant cellular debris constituting the smegma (Figs. 5 and 6). The outer, parietal surface of the preputium is folded and covered densely with hair (Figs. 2, 5, and 6). The epidermis is a stratified squamous keratinized epithelium with a distinct layer of melanocytes (Fig. 6). No keratinized spines or papillary buds were found.

Baculum Development in *Pipistrellus pipistrellus*

In the juvenile and subadult bats, the whole baculum consists of woven bone. While the distal part of the shaft with the forked tip seems to be

Fig. 3. Corresponding µCT virtual section (left; iodine stained; taken from overview scan) and Giemsa surface-stained ground section (right) of a *P. pipistrellus* (NMW 52177) penis in ventral view. The visible portion of the baculum (ba) shows woven bone (wb) with densely packed osteocyte lacunae in the periphery, and lamellar bone (lb) with sparse osteocytes around the medullary cavity (mc). ba: baculum, cc: corpora cavernosa, cs: corpus spongiosum, en: entheses, fm: fatty marrow (with blood vessels in between), la: blood lacunae (in the corpora cavernosa), lb: lamellar bone, mc: medullary cavity within the baculum (with fatty bone marrow (fm) and blood vessels), po: periosteum, pr: preputium, ps: preputial sac, ta: tunica albuginea (of the corpora cavernosa), tr: trabeculae (in the corpora cavernosa), ur: urethra, wb: woven bone.

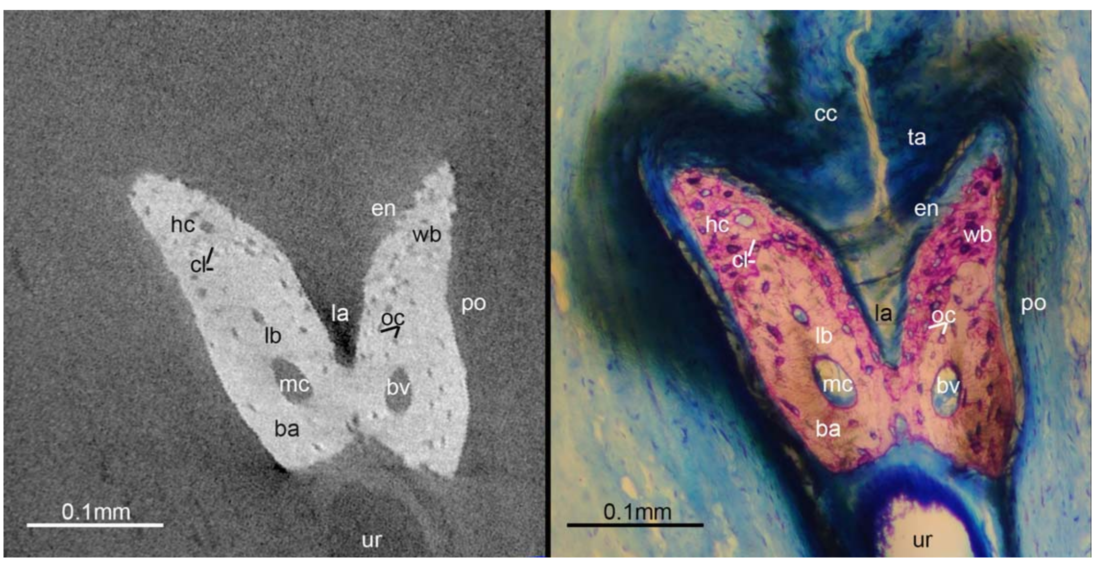

Fig. 4. Corresponding µCT virtual section (left; iodine stained; detail scan of the proximal baculum and surrounding soft tissue) and Giemsa surface-stained ground section (right) of a *P. pipistrellus* (NMW 66144) penis in dorsal view. The visible portion of the baculum (ba) shows woven bone (wb) with densely packed osteocyte lacunae in the periphery, and lamellar bone (lb) with sparse osteocytes separated by a distinct cement line (cl); around the medullary canal (mc). ba: baculum, bv: blood vessels, cc: corpora cavernosa, cl: cement line, en: entheses, hc: haversian canal, la: blood lacunae (in the corpora cavernosa), lb: lamellar bone, mc: medullary canal (within the baculum) with blood vessels, oc: osteocytes, po: periosteum, ta: tunica albuginea (of the corpora cavernosa), ur: urethra, wb: woven bone.

Fig. 5. MicroCT 3D surface rendering of the baculum (ba), urethra (ur), glans penis (gl), and corpora cavernosa (cc) with 3D volume rendering and 2D virtual section of the penis in lateral view (left; iodine stained; overview scan) and Giemsa surface-stained ground section (right, focus stack of several photographs) of a *P. pipistrellus* (NMW 66144) penis in ventral view. Showing the position of the distal tip of the baculum (ba) at the external urethral orifice (uo; left) and the bone structure of the baculum shaft (ba; right). ac: accessory swelling tissue, ba: baculum, cc: corpora cavernosa, cl: cement line, gl: glans penis, ha: hair, lb: lamellar bone, mc: medullary canal (within the baculum) with blood vessels, pr: preputium, ps: preputial sac, uo: external urethral orifice, ur: urethra, wb: woven bone.

mostly developed, the proximal base of the baculum is distinctly different from the appearance in adults (Fig. 7). The branches are shorter and not as broad as in adult specimens. The woven bone at the base contains single, large, densely packed, round or cubic osteocytes, that resemble chondrocytes (Fig. 7A). However, the corresponding µCT-images show a mineralized extracellular matrix. In some of the bacula from subadult bats ($n = 6$) and one from a juvenile, a primary medullary cavity was found where the branches of the base merge into the shaft, sometimes with a large opening to the ventral side of the bone (Fig. 7B), sometimes expanding into the distal part of the branches. The other bacula (juvenile $n = 4$, subadult $n = 1$) only had a small primary medullary cavity, where the branches of the base merge into the shaft.

DISCUSSION

By verifying histomorphological findings on µCT-images with light microscopic evaluation of serial surface-stained ground sections, correlative imaging of museum specimens enabled us to study *Pipistrellus* penes in greater detail and in more specimens than would a single technique. Some tissue properties, like discriminating woven from lamellar bone by the shape and size of osteocytes, can readily be studied on virtual sections from µCT-images alone (Fig. 4). Soft tissues can be distinguished in µCT-images of iodine stained *P. pipistrellus* and *P. nathusii* penes by different gray values, representing different radiodensities, determined by the extent to which the tissues take up iodine (Figs. 2–5).

For other findings, like the identification of fatty marrow or of cement lines, the comparison of µCT-images with ground sections of the same individual in the same section plane and orientation was necessary (Figs. 2–4). The ground sections showed more detailed histological traits in the soft tissue, in addition to what we found with µCT. After thus calibrating our µCT-images, these structures could be found and confidently interpreted in µCT-images of other specimens, even of different species. Additionally, 3D-renderings of µCT-images provide a better understanding of the overall shape of *Pipistrellus* bacula and facilitate comparisons between species (Figs. 1, 5, and 7).

We originally evaluated the micromorphology of the baculum to find characters that could

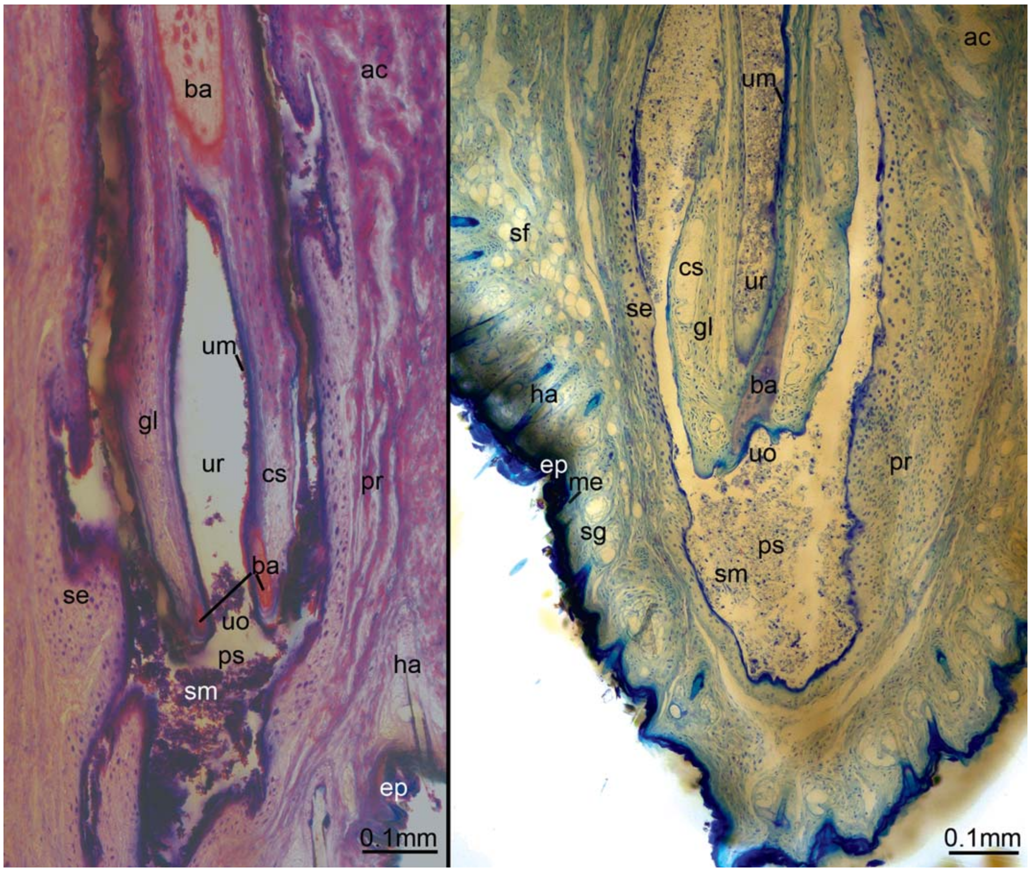

Fig. 6. Giemsa surface-stained ground sections of the distal tip of the penis in two different *P. pipistrellus* specimens (left: NMW 66144, right: NMW 52177). Dorsal view (left) and ventral view (right) show how the distal tip of the baculum encases the dorsal half of the external urethral orifice. ac: accessory swelling tissue, ba: baculum, cl: cement line, cs: corpus spongiosum, ep: epidermis, gl: glans penis, ha: hair, lb: lamellar bone, mc: medullary canal (within the baculum) with blood vessels, me: melanocytes, pr: preputium, ps: preputial sac, se: stratified epithelium, sf: subcutaneous fat, sg: sebaceous gland, sm: smegma, um: urethral mucosa, uo: external urethral orifice, ur: urethra, wb: woven bone.

potentially be used for differentiating *Pipistrellus* species (Herdina et al., 2014). Differences in dorsoventral curve shape (Fig. 1), as found between the specimens of *Pipistrellus pipistrellus*, *P. pygmaeus*, and *P. hanaki*, seem to represent only individual variation. The location and length of the medullary canal, Volkmann's canals, and nutrient foramina in *Pipistrellus pipistrellus*, *P. pygmaeus*, *P. hanaki*, and *P. nathusii* exhibit much more individual variation than in the *Plecotus* species examined previously (Herdina, 2008; Herdina et al., 2010a). This variation ranges from specimens without any medullary canals to specimens with large cavities in the branches of the proximal base, and extremely large nutrient foramina. Therefore these characters do not appear to be usable in *Pipistrellus* species identification.

The prevalence of a secondary medullary cavity with fatty marrow in mammalian bacula is unclear. The occurrence of a canal or cavity filled with connective tissue and blood vessels in the baculum has been reported in the parti-coloured bat *Vespertilio murinus* (Gilbert, 1892) and in various rodents (Gilbert, 1892; Glucksmann and Cherry, 1972; von Ihering, 1885; Retterer, 1887). Bone marrow, without further description, was reported in the baculum of mice (Iguchi et al., 1990; Iguchi and Ohta, 1996; Deveci et al., 2009; Yildiz et al., 2010) and rats (Yoshida and Kadota, 1980). The occurrence of fatty bone marrow was only mentioned in the baculum of rats (Retterer, 1887). The fatty bone marrow found in the medullary cavity of the baculum, together with cement lines as evidence of bone remodeling, identifies the baculum as a mature bone.

The histomorphological structure of the lamellar bone with a central canal and small Volkmann's canals but no Haversian canals resembles the structure of a single osteon. Thus, it appears that the lamellar portion of the baculum develops like a single secondary osteon in all of the *Plecotus* (Herdina, 2008; Herdina et al., 2010a) and *Pipistrellus* species we have studied (Fig. 7). However, the baculum in the studied bat species (Figs. 2–5) is not a single-osteon bone, because of the presence of woven bone around the lamellar

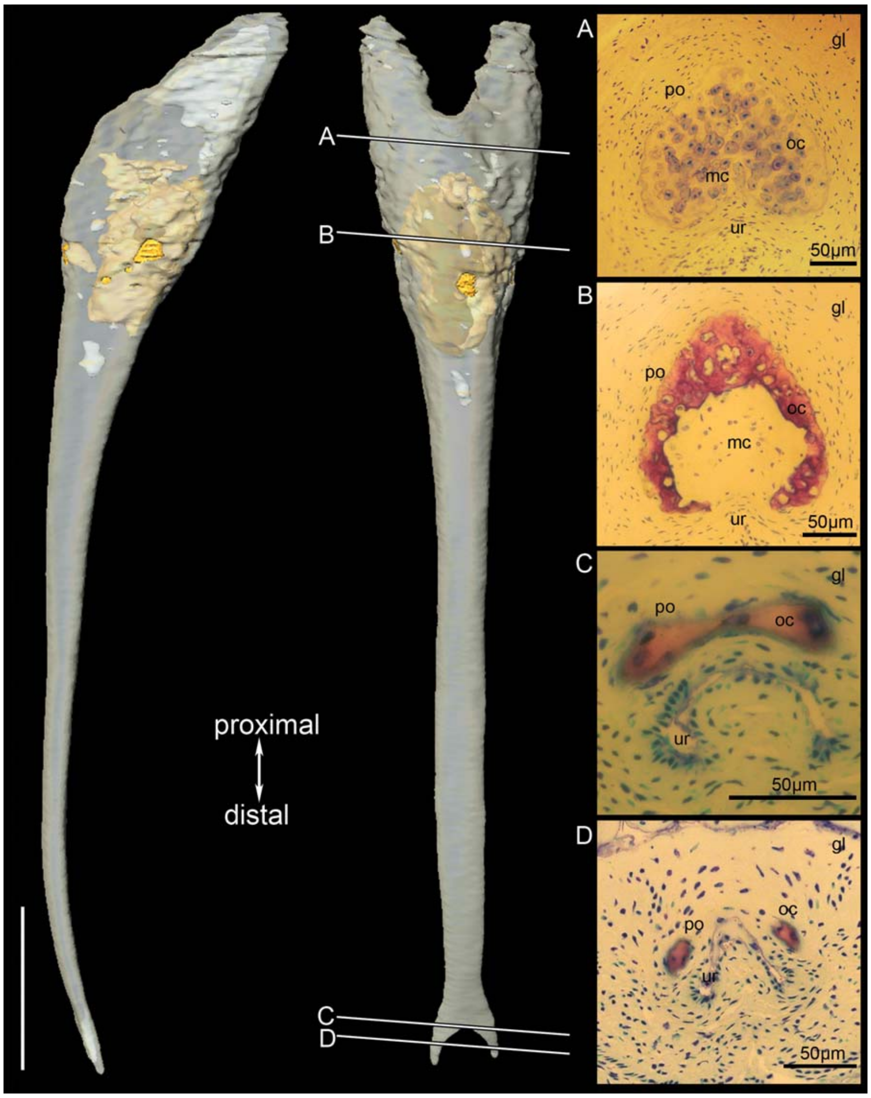

Fig. 7. Baculum 3D surface renderings, medullary cavity and canals in orange; left: lateral view, middle: dorsal view; projected length: 1.3mm. Scale bar: 200µm. Slightly oblique ground cross-sections (right, A-D; Giemsa stained) of juvenile *P. pipistrellus* (NMW 66530). A: base of the baculum with osteocytes (oc) resembling chondrocytes and a small medullary canal (mc). B: distal part of the baculum base with large primary medullary cavity (mc). C and D: distal end of the baculum where the forked baculum tip surrounds the dorsal half of the external urethral orifice. gl: glans penis, mc: medullary cavity/canal, oc: osteocytes, po: periosteum, ur: urethra.

portion and because of the occurrence of a secondary medullary cavity filled with fatty marrow, although such bones have been found in other vertebrates, for example the femur of the Japanese fire-bellied salamander *Cynops pyrrhogaster* (Urschitz, 1982) and other amphibians (e.g. Rana esculenta; Demeter and Mátyás, 1928).

Ground sections of *Pipistrellus pipistrellus* bacula and µCT-images of the bacula of all the species studied complement the results of our earlier studies on *Plecotus* baculum histomorphology (Herdina, 2008; Herdina et al., 2010a), and results of this study on soft tissue histomorphology corroborate the results of previous studies of bat penes (Matthews, 1937; Ryan, 1991a, 1991b; Herdina, 2008; Herdina et al., 2010a). The small glans and the thick preputium, containing accessory swelling tissue, of *P. pipistrellus s.l.* (Figs. 2, 3, 5, and 6) were described by Matthews (1937), who called this swelling tissue the accessory corpus cavernosum (citing Ercolani, 1868, who named it in *Vespertilio* [=*Myotis*]). The thick preputium might effect coital locking, as proposed for *Myotis lucifugus* by Wimsatt and Kallen (1952). Contrary to findings in some other bat species (Vamburkar, 1958; Ryan, 1991a; Crichton and Krutzsch, 2000; Armstrong, 2005; Cryan et al., 2012), we did not find penile spines on the penes of the species studied.

Our results provide histomorphological support for two hypotheses of baculum function. 1) The baculum forms a functional unit with the corpora cavernosa (Figs, 2–4), facilitating force transfer from the tip of the penis to the corpora cavernosa and increasing overall flexural stiffness of the glans and shaft of the penis (Kelly, 2000; Herdina et al., 2015). 2) The baculum protects the distal part of the urethra and the external urethral orifice (Figs. 5–7) from compression during copulation (Dixson, 1995; Herdina et al., 2015). The forked tip of the baculum encloses the upper half of the external urethral orifice in all the *Pipistrellus* species studied.

Our preliminary results on baculum development in *Pipistrellus pipistrellus* show that the distal part of the baculum reaches its adult shape before the proximal part (Fig. 7). We did not study young enough individuals to confirm if a cartilage precursor to the baculum exists in this species. However, the woven bone tissue in the base of the juvenile and subadult bats, with large round osteocytes resembling chondrocytes (Fig. 7A), could be chondroid bone (as described by Schaffer, 1930). At least two juvenile specimens were not yet capable of flight, while the subadult bats we studied were already capable of flight and had probably already left the maternity colonies in which they were born. The different states of medullary cavity development we found suggest an invasion of blood vessels from the ventral side of the baculum, where the branches of the base meet the shaft (Fig. 7B).

Variability in the innervation and the morphology of medullary canals of bone is a well-known phenomenon (Usener, 1966). The different degree of variability of the morphology of the medullary canals in the bacula of bat species of the genera *Pipistrellus* and *Plecotus* is interesting because it may imply differences in ontogenetic plasticity. To our knowledge, the ontogeny of the baculum in bats has not been studied histologically, but only in dissected or macerated penes (Vlček, 1967; Maeda, 1978a, 1978b; Smirnov and Tsytsulina, 2003).

CONCLUSION

Correlative 2D and 3D-imaging can be especially useful for studying valuable museum specimens. High-resolution μCT-images can be obtained without modifying or damaging the specimens, allowing a larger number of samples to be studied, even if the study organism is rare in scientific collections. Combining μCT-imaging with specialized histomorphological techniques like surface-stained ground sections enables accurate identification of histological structures in the μCT-images. It also creates an independent data set that can be useful in further studies. Thus correlating a versatile 3D-image and virtual 2D-sections from μCT-scans with ground section surfaces of the same specimen in different orientations and combinations becomes possible, even long after the specimen has been returned or processed histologically.

ACKNOWLEDGMENTS

The authors would like to thank Ivan Horáček, Vladimír Hanák, and Adrienne Hilgers for fruitful discussions on the subject. We are grateful to Gerd Müller (Dept. of Theoretical Biology, University of Vienna), Karl Großschmidt (Bone and Biomaterials Research, Institute of Histology and Embryology, Medical University of Vienna) and Robert Černý (Dept. of Zoology, Charles University) for providing resources of their departments; and to Frank Zachos (Natural History Museum Vienna) and Steven van der Mije (Naturalis Biodiversity Center, Leiden) for granting us access to specimens. The authors thank Beate Wallner, Astrid Haase, and Barbara Rendl for assistance in preparing ground sections; Pavel Hulva for molecular genetic species identification; and Friederike Spitzenberger and two anonymous reviewers for helpful comments on the manuscript. Author contributions: The project was developed by Anna Nele Herdina, Helge Hilgers, Barbara Herzig-Straschil, Brian D. Metscher and Hanns Plenk. MicroCT-imaging and iodine staining were done by Brian D. Metscher and Anna Nele Herdina. Anna Nele Herdina measured and segmented μCT-images. Hanns Plenk and Anna Nele Herdina made, stained, and photographed ground sections. Petr Benda, Peter H. C. Lina, and Barbara Herzig-Straschil contributed the specimens. All authors contributed ideas and discussed the results. The manuscript was written by Anna Nele Herdina, Brian D. Metscher, and Hanns Plenk.

LITERATURE CITED

Albayrak I, Özen AS, Kitchener AC. 2008. A contribution to the age-class determination of *Martes foina* Erxleben, 1777 from Turkey (Mammalia: Carnivora). Turk J Zool 32:147–153.

Armstrong KN. 2005. A description and discussion of the penile morphology of *Rhinonicteris aurantius* (Gray, 1845) (Microchiroptera: Hipposideridae). Aust Mammal 27:161–167.

Banks WJ. 1993. Applied Veterinary Histology. St. Louis: Mosby Year Book. 527 p.

Benjamin M, Evans EJ, Coop L. 1986. The histology of tendon attachments to bone in man. J Anatomy 149:89–100.

Burt WH. 1936. A study of the baculum in the genera *Perognathus* and *Dipodomys*. J Mammal 17:145–156.

Callery H. 1951. Developement of the os genitale in the golden hamster, *Mesocricetus* (*Cricetus*) *auritus*. J Mammal 32:204–207.

Crichton EG, Krutzsch PH. 2000. Reproductive Biology of Bats. London: Academic Press. 510 p.

Cryan PM, Jameson JW, Baerwald EF, Willis CKR, Barclay RMR, Snider EA, Crichton EG. 2012. Evidence of late-summer mating readiness and early sexual maturation in migratory tree-roosting bats found dead at wind turbines. PLoS One 7:e47586.

Davidson-Watts I, Walls S, Jones G. 2006. Differential habitat selection by *Pipistrellus pipistrellus* and *Pipistrellus pygmaeus* identifies distinct conservation needs for cryptic species of echolocating bats. Biol Conserv 133:118–127.

Demeter G, Mátyás J. 1928. Mikroskopisch vergleichend-anatomische Studien an Röhrenknochen mit besonderer Rücksicht auf die Unterscheidung menschlicher und tierischer Knochen. Z Anat Entwicklungsgesch 87:45–99.

Deveci E, Nergiz Y, Inalöz S, Akkuş M, Ketani MA, Ersay AR. 2009. The effect of tamoxifen on the neonatal development of rat penis. Turk J Med Sci 28:375–382.

Dixson AF. 1995. Baculum length and copulatory behaviour in carnivores and pinnipeds (Grand Order Ferae). J Zool (London) 235:67–76.

Ercolani GB. 1868. Dei tessuti e degli organi erettili. Mem dell'accademia dei scienze dell'istituto di Bologna 8:281–362.

Friley CE Jr. 1949. Use of the baculum in age determination of Michigan beaver. J Mammal 30:261–267.

Gilbert T. 1892. Das Os priapi der Säugethiere. Morphol Jahrb 18:805–813.

Glucksmann A, Cherry CP. 1972. The hormonal induction of an os clitoridis in the neonatal and adult rat. J Anatomy 112: 223–231.

Handschuh S, Baeumler N, Schwaha T, Ruthensteiner B. 2013. A correlative approach for combining microCT, light and transmission electron microscopy in a single 3D scenario. Front Zool 10:44.

Herdina AN. 2008. Light microscopy of the penis bone (baculum) in the *Plecotus* species (Chiroptera) in Austria [M.Sc. thesis]: Department of Theoretical Biology, Faculty of Life Sciences, University of Vienna, Austria. 74 p.

Herdina AN, Herzig-Straschil B, Hilgers H, Metscher BD, Plenk Jr. H. 2010a. Histomorphology of the penis bone (baculum) in the gray long-eared bat *Plecotus austriacus* (Chiroptera, Vespertilionidae). Anat Rec 293:1248–1258.

Herdina AN, Plenk Jr. H, Pokorny P, Hilgers H, Herzig-Straschil B, Metscher BD. Looking at baculum function from a histomorphological perspective. In: Horáček I, Benda P, editors; 2010b. p 169.

Herdina AN, Hulva P, Horáček I, Benda PP, Metscher BD. 2014. MicroCT imaging reveals morphometric baculum differences for discriminating the cryptic species *Pipistrellus pipistrellus* and *P.* pygmaeus. Acta Chiropterologica 16:157–168.

Herdina AN, Kelly DA, Jahelková H, Lina PHC, Horáček I, Metscher BD. 2015 Testing hypotheses of bat baculum function with 3D models derived from microCT. J Anat 226:229–235.

Hill JL, Harrison DL. 1987. The baculum in the Vespertilioninae (Chiroptera: Vespertilionidae) with a systematic review, a synopsis of *Pipistrellus* and *Eptesicus*, and the descriptions of a new genus and subgenus. Bull Br Mus (Nat Hist) Zool 52:225–305.

Hulva P, Fornůsková A, Chudárková A, Evin A, Allegrini B, Benda P, Bryja J. 2010. Mechanisms of radiation in a bat group from the genus *Pipistrellus* inferred by phylogeography, demography and population genetics. Mol Ecol 19:5417–5431.

Iguchi T, Irisawa S, Uesugi Y, Kusunoki S, N T. 1990. Abnormal development of the os penis in male mice treated neonatally with tamoxifen. Acta Anat (Basel) 139:201–208.

Iguchi T, Ohta Y. 1996. Cellular effects of early exposure to tamoxifen. In: Kellen JA, editor. Tamoxifen: Beyond the antiestrogen. Birkhäuser, Boston. pp 179–200.

Kelly DA. 2000. Anatomy of the baculum-corpus cavernosum interface in the Norway rat (*Rattus norvegicus*), and implications for force transfer during copulation. J Morphol 244:69–77.

Maeda K. 1978a. Baculum of the Japanese large noctule, *Nyctalus lasiopterus aviator* Thomas, 1911. Acta Anat Nipponica 53:447–453.

Maeda K. 1978b. Baculum of the little tube-nosed bats, *Murina aurata* Milne-Edwards 1872. J Mammal Soc Japan 7:224–227.

Matthews LH. 1937. The form of the penis in the British Rhinolophid bats, compared with that in some of the Vespertilionid bats; and the female sexual cycle in the British horse-shoe bats, *Rhinolophus ferrum-equinum insulanus* Barrett-Hamilton and *R. hipposideros minutus* Montagu. Trans Zool Soc London, Part 4 23:213–266.

Meisenheimer J. 1921. Geschlecht und Geschlechter im Tierreiche: Verlag von Gustav Fischer, Jena. 896 p.

Metscher BD. 2009a. MicroCT for comparative morphology: Simple staining methods allow high-contrast 3D imaging of diverse non-mineralized animal tissues. BMC Physiol 9:11.

Metscher BD. 2009b. MicroCT for developmental biology: A versatile tool for high-contrast 3D imaging at histological resolutions. Dev Dyn 238:632–640.

Metscher BD. 2011. X-ray microtomographic imaging of intact vertebrate embryos. Cold Spring Harb Protoc 12: 1462–1471.

Miller EH, Stewart ARJ, Stenson GB. 1998. Bacular and testicular growth, allometry, and variation in the harp seal (*Pagophilus groenlandicus*). J Mammal 79:502–513.

Murakami R, Mizuno T. 1984. Histogenesis of the os penis and os clitoridis in rats. Dev Growth Diff 26:419–426.

Murakami R, Mizuno T. 1986. Proximal-distal sequence of development of the skeletal tissues in the penis of rat and the inductive effect of epithelium. J Embryol Exp Morphol 92: 133–143.

Patterson BD. 1983. Baculum-body size relationships as evidence for a selective continuum on bacular morphology. J Mammal 64:496–499.

Patterson BD, Thaeler CSJ. 1982. The mammalian baculum: Hypothesis on the nature of bacular variability. J Mammal 63:1–15.

Petrides GA. 1950. The determination of sex and age ratios in fur animals. Am Midland Nat 43:355–382.

Plenk H Jr. 1986. The microscopic evaluation of hard tissue implants. In: Williams DF, editor. Techniques of Biocompatibility Testing. CRC Press: Boca Raton, Florida. pp 35–81.

Retterer E. 1887. Note sur le développement du penis et du squelette du gland chez certains rongeurs. Comptes Rendus Hebdomadaires des Seances et Memoires de la Soc de Biologie (C R Soc Biol) tome 4 (39 de la collection):496–498.

Ruth EB. 1934. The os priapi: A study in bone development. The Anat Rec 60:231–249.

Ryan JM. 1991a. Comparative morphology of the glans penis in *Molossus promops* and *eumops* (Chiroptera, Molossidae). Bull Am Mus Nat Hist 206:122–137.

Ryan JM. 1991b. Morphology of the glans penis in four genera of Molossid bats (Chiroptera: Molossidae). J Mammal 72:658–668.

Schaffer J. 1930. Die Stützgewebe. In: von Möllendorff W, editor. Handbuch der mikroskopischen Anatomie des Menschen. Springer: Berlin. pp 1–390.

Schwery O, Köhnemann BA, Michler FU, Brinkmann W. 2011. Morphometrical characterisation of a raccoon population from Müritz National Park (Germany) by means of the os baculum. Beiträge zur Jagd-und Wildforschung 36:605–617.

Smirnov DG, Tsytsulina K. 2003. The ontogeny of the baculum in *Nyctalus noctula* and *Vespertilio murinus* (Chiroptera: Vespertilionidae). Acta Chiropterologica 5:117–123.

Spotorno AE. 1992. Parallel evolution and ontogeny of simple penis among new world cricetid rodents. Am Soc Mammal 73: 504–514.

Thomas O. 1915. The penis bone, or'' baculum,'' as a guide to the classification of certain squirrels. Ann Mag Nat Hist 8: 383–387.

Topál G. 1958. Morphological studies on the os penis of bats in the Carpathian Basin. Ann Hist Nat Mus Hungarica 50:331–342.

Urschitz M. 1982. Stoffwechselaktivität des Knochengewebes bei verschiedenen Vertebratenspecies [PhD thesis]: University of Vienna, Austria.

Usener I. 1966. Ausformung der menschlichen Humerusmarkhöhle und ihre Variabilität. Gegenbaurs Morphol Jahrbuch 108:607–623.

Vamburkar SA. 1958. The male genital tract of the Indian megachiropteran bat *Cynopterus sphinx gangeticus* Proc Zool Soc London 130:57–77.

Vlček M. 1967. Bakulum netopýrů rodu *Myotis* [M.Sc. thesis]: Charles University, Prague, Czech Republic. 94 p.

von Ihering H. 1885. Zur Kenntnis der brasilianischen Mäuse und Mäuseplagen. Kosmos - Zeitschrift für die gesamte Entwickelungslehre 2:423–437.

Weiss DA, Rodriguez Jr. E, Cunha T, Menshenina J, Barcellos D, Chan LY, Risbridger G, Baskin L, Cunha G. 2012. Morphology of the external genitalia of the adult male and female mice as an endpoint of sex differentiation. Mol Cell Endocrinol 354:94–102.

Wimsatt WA, Kallen FC. 1952. Anatomy and histophysiology of the penis of a vespertilionid bat, *Myotis lucifugus lucifugus*, with particular reference to its vascular organisation. J Morphol 90:415–465.

Yildiz D, Bolat D, Karahan S. 2010. The morphology of the os penis in the adult mouse. J Animal Vet Adv 9:1913–1917.

Yoshida H, Kadota A. 1980. Effects of testosterone propionate on neonatal and prepubertal development of os penis in male rats. J of Exp Anim Sci 29:49–43.